New Perspectives for Nonlinear Depth-inversion of the Nearshore Using Boussinesq Theory

Kévin Martins[1], Philippe Bonneton[1], Olivier De Viron[2], Ian L Turner[3], Mitchel D Harley[3], and Kristen Splinter[3]

[1]Univ. Bordeaux
[2]La Rochelle University
[3]UNSW Sydney

November 26, 2022

Abstract

Accurately mapping the evolving bathymetry under energetic wave breaking is challenging, yet critical for improving our understanding of sandy beach morphodynamics. Though remote sensing is one of the most promising opportunities for reaching this goal, existing depth-inversion algorithms using linear approaches face major theoretical and/or technical issues in the surf zone, limiting their accuracy over this region. Here, we present a new depth-inversion approach relying on Boussinesq theory for quantifying nonlinear dispersion effects in nearshore waves. Using high-resolution datasets collected in the laboratory under diverse wave conditions and beach morphologies, we demonstrate that this approach results in enhanced levels of accuracy in the surf zone (errors typically within 10%) and presents a major improvement over linear methods. The new nonlinear depth-inversion approach provides significant prospects for future practical applications in the field using existing remote sensing technologies, including continuous lidar scanners and stereo imaging systems.

New Perspectives for Nonlinear Depth-inversion of the Nearshore Using Boussinesq Theory

Kévin Martins[1,2], Philippe Bonneton[1], Olivier de Viron[3], Ian L. Turner[2], Mitchel D. Harley[2], Kristen Splinter[2]

[1]Univ. Bordeaux, CNRS, Bordeaux INP, EPOC, UMR 5805, F-33600 Pessac, France
[2]Water Research Laboratory, School of Civil and Environmental Engineering, UNSW Sydney, 110 King Street, Manly Vale, NSW, 2093, Australia
[3]La Rochelle University, CNRS, LIENSs, UMRi 7266, 17000 La Rochelle, France

Key Points:

- A new depth-inversion approach for the nearshore and surf zone is proposed, based on a Boussinesq theory for quantifying nonlinear dispersion effects
- Unprecedented levels of accuracy (typically within 10%) are obtained in the surf zone over both planar and barred beaches
- This is a substantial improvement over the existing linear wave theory method, which commonly overestimates depths by 40% or more in surf zones, and up to 80% close to the shoreline

Corresponding author: Kévin Martins, kevin.martins@u-bordeaux.fr

Abstract

Accurately mapping the evolving bathymetry under energetic wave breaking is challenging, yet critical for improving our understanding of sandy beach morphodynamics. Though remote sensing is one of the most promising opportunities for reaching this goal, existing depth-inversion algorithms using linear approaches face major theoretical and/or technical issues in the surf zone, limiting their accuracy over this region. Here, we present a new depth-inversion approach relying on Boussinesq theory for quantifying nonlinear dispersion effects in nearshore waves. Using high-resolution datasets collected in the laboratory under diverse wave conditions and beach morphologies, we demonstrate that this approach results in enhanced levels of accuracy in the surf zone (errors typically within 10%) and presents a major improvement over linear methods. The new nonlinear depth-inversion approach provides significant prospects for future practical applications in the field using existing remote sensing technologies, including continuous lidar scanners and stereo imaging systems.

Plain Language Summary

The coastal science community currently lacks insights into the morphological evolution of sandy beaches, including rapid changes that occur during storms. This is, to a large extent, explained by the difficulty to monitor the seabed elevation under such conditions in a region of the nearshore where high-energy waves break. If a relationship can be established between observed wave dynamics at the surface and the water depth below, remote-sensing technology presents a promising opportunity to reach this goal since it requires no physical interaction with the water environment. However, the existing algorithms to retrieve the water depth rely on the linear wave dispersion relation, which fails at describing the non-linear dynamics of shoaling and breaking waves. Here, we develop a new depth-inversion approach based on a Boussinesq theory, which better describes such dynamics. Using a range of wave conditions and beach morphologies, we demonstrate that our approach results in significant improvement compared to the classic approaches, achieving typical accuracy within 10% in regions of the nearshore where waves break. The new nonlinear depth-inversion approach provides very promising prospects for future practical applications in the field using, for instance, high-resolution datasets collected with lidar scanners or stereo imaging systems.

1 Introduction

Understanding the temporal evolution of the nearshore bathymetry is critical to a wide range of applications including forecasting of coastal hazards, the morphological evolution of the sea/land interface and naval operations. However, mapping with sufficient accuracy and resolution the water depth along wave-dominated coastlines remains very challenging, especially in the region of energetic wave breaking in the surf zone. Remote-sensing technology, combined with depth-inversion algorithms, presents a promising opportunity to achieve this goal while minimizing risks associated with human intervention or the substantial challenges of installing and maintain in situ measurement equipment.

When currents are neglected, the linear wave dispersion relation provides a direct link between the spatial and temporal information of a surface wave field approaching the shore:

$$\omega^2 = g\kappa_L \tanh(\kappa_L h), \tag{1}$$

where $\omega = 2\pi f$ is the angular wave frequency, g is the acceleration of gravity, κ_L denotes the wavenumber magnitude[1] and h is the mean water depth. Depth-inversion algorithms such as *cBathy* (Holman et al., 2013) use this relationship (Eq. 1) to infer depth from

[1] $\kappa = |\vec{k}|$ here denotes the (single-valued) magnitude of the wavenumber vector $\vec{k}$

wave dispersive properties extracted from optical imagery (*e.g.*, see Stockdon & Holman, 2000; Plant et al., 2008; Holman & Bergsma, 2021). In intermediate water depths, Eq. 1 accurately describes the dispersive properties of low-amplitude wave fields so that typical errors on the water depth estimated with an algorithm like *cBathy* can be as low as 10% (*e.g.*, see Dugan et al., 2001; Holland, 2001; Brodie et al., 2018). Closer to the breaking point and in surf zones, however, nonlinear amplitude dispersion effects intensify and significant deviations of dominant wavenumbers from the linear dispersion are expected (Thornton & Guza, 1982; Elgar & Guza, 1985b; Herbers et al., 2002; Martins, Bonneton, & Michallet, 2021). The present approaches based on optical imagery also suffer from technical limitations such as spurious phase shifts induced by breaking waves (Bergsma et al., 2019). These issues significantly affect the stability and accuracy of remotely-sensed wave dispersive properties, leading to errors on the water depths typically between 50-600% near and inside the surf zone (*e.g.*, see Holland, 2001; Catalán & Haller, 2008; Bergsma et al., 2016; Brodie et al., 2018). New approaches are thus required in order to consistently reduce this error and make it possible to monitor the morphological evolution of sandy beaches.

Technologies such as lidar scanners (Brodie et al., 2015; Martins et al., 2017; Fiedler et al., 2021) and stereo-video imagery (de Vries et al., 2011; Bergamasco et al., 2017) have seen major developments over the last decade and now allow the collection of accurate measurements of the sea-surface elevation in nearshore areas. By making information on wave heights directly accessible, these technologies offer the potential to substantially improve bathymetry inversion in the surf zone and right up to the shoreline. However, a universal nonlinear dispersion relation for shoaling and breaking waves is still lacking (for the most recent review refer: Catalán & Haller, 2008). Here, we describe a new depth-inversion method that relies on the stochastic Boussinesq theory of Herbers et al. (2002) to quantify nonlinear frequency and amplitude dispersion effects within both the shoaling and breaking wave regions. The new approach utilises high-resolution datasets of free surface elevation and is designed so that it can be applied in the field with any technology collecting such data (*e.g.*, lidar scanners, stereo imagery systems). Suitable test datasets collected in the laboratory over both planar and barred beaches are used to demonstrate that the new nonlinear depth-inversion approach consistently outperforms the linear method (Eq. 1), opening new perspectives for practical depth-inversion of surf zones in the field.

2 Methods

2.1 Experimental Datasets

The new Boussinesq depth-inversion approach is developed then evaluated using high-resolution surface elevation datasets collected in the laboratory. Here, the objective is to mimic under controlled conditions the field situation in which similar datasets can now be routinely collected using existing remote-sensing technologies. Though lidars presently offer the most robust and practical solution for collecting highly-resolved surface elevation data in the field, the approach presented is applicable to any technology capable of collecting such data (*e.g.*, stereo imagery systems).

We consider three specific series of experiments, which covered a relatively wide range of wave conditions and beach morphologies. The experiments of van Noorloos (2003) were performed over a 1:35 planar beach in the 40 m-long wave flume at Delft University of Technology (Fig. 1; see also van Dongeren et al., 2007). A second planar beach case originates from the Gently sLOping Beach Experiment (GLOBEX) performed over a mildly-sloping concrete beach (1:80) specifically built in a 110 m-long wave flume in Delft, the Netherlands (Fig. 1; see also Ruessink et al., 2013). Finally, we use a 30 min-long sequence extracted from the experiments performed over a mobile bottom in the 36 m-long LEGI flume and described in Michallet et al. (2011). The sediment for this latter experiment was chosen such that the Shields and Rouse numbers were of similar magnitude as those found in natural environments (Grasso et al., 2009). The beach profile exhibited a pronounced sandbar that migrated landward by about 2.5 m during the wave sequence (Fig. 1).

For the planar beach cases, we concentrate on the most energetic tests performed with irregular waves. For the experiments of van Noorloos (2003), this corresponds to the C_3 wave test, characterized by a significant wave height $H_{m0} = 0.1\,\mathrm{m}$ and peak frequency $f_p = 0.5\,\mathrm{Hz}$. For GLOBEX, this corresponds to the A2 wave test ($H_{m0} = 0.2\,\mathrm{m}$; $f_p = 0.444\,\mathrm{Hz}$). During the experiments of Michallet et al. (2011), the conditions consisted of irregular waves characterized by $H_{m0} = 0.16\,\mathrm{m}$ and $f_p = 0.4\,\mathrm{Hz}$. The free surface elevation ζ was collected at high spatial resolution, which generally varied across the direction of wave propagation (Fig. 1).

2.2 Estimating and Predicting Wave Dominant Dispersive Properties

In the nearshore region, nonlinear interactions between triads of frequencies lead to the growth of forced high-frequency components (Phillips, 1960; Freilich et al., 1984; Elgar & Guza, 1985a; Herbers et al., 2000). Both free and forced wave components then co-exist at a given frequency, causing deviations of dominant wavenumbers from the linear wave dispersion relation (Elgar & Guza, 1985b; Herbers et al., 2002; Martins, Bonneton, & Michallet, 2021). In practice, dominant wavenumber spectra can be estimated from cross-spectral analyses between adjacent pressure (Elgar & Guza, 1985b; Herbers et al., 2002) or wave gauges (Martins, Bonneton, & Michallet, 2021). In the present 1D configuration, we follow the procedure described in Martins, Bonneton, and Michallet (2021) to estimate the dominant wavenumber spectra κ_{obs} across the experiments. A maximum distance of $0.3L_p$ was allowed between adjacent wave gauges for the cross-spectral analysis, where L_p is the peak wavelength predicted by the linear wave dispersion relation (Eq. 1).

Dominant wavenumber spectra κ_{rms} are then estimated from the surface elevation ζ using the Boussinesq theory of Herbers et al. (2002):

$$\kappa_{rms}(\omega) = \frac{\omega}{\sqrt{gh}}\sqrt{1 + h\gamma_{fr,1}(\omega) + h^2\gamma_{fr,2}(\omega) - \frac{1}{h}\gamma_{am}(\omega)}, \tag{2}$$

with

$$\begin{aligned} \gamma_{fr,1}(\omega) &= \frac{\omega^2}{3g} && (3)\\ \gamma_{fr,2}(\omega) &= \frac{\omega^4}{36g^2} && (4)\\ \gamma_{am}(\omega) &= \frac{3}{2E(\omega)}\int_{-\infty}^{\infty} \mathrm{Re}\{B(\omega', \omega-\omega')\}d\omega', && (5) \end{aligned}$$

where E and B are the spectral and bispectral densities of ζ respectively, and Re{.} denotes the real part. Further details on the computation of cross-spectral, spectral and bispectral estimates can be found in the Supporting Information. In Eq. 2, the leading-order term corresponds to the wavenumber for non-dispersive shallow-water waves. Terms with $\gamma_{fr,1}$ and $\gamma_{fr,2}$ are second and fourth-order frequency dispersion terms, respectively, while γ_{am} is a second-order amplitude dispersion term. Compared to the original expression for κ_{rms} given by Herbers et al. (2002, their Eq. 12), we kept the fourth-order frequency term $\gamma_{fr,2}$ in order to improve the linear dispersive properties of the Boussinesq approximation. Each term was also here expressed in a way that h remains isolated, which facilitates the depth-inversion procedure (Section 2.3). The Boussinesq approximation of κ_{rms} (Eq. 2) was derived assuming that the wave field is weakly nonlinear, weakly dispersive, and that these effects are of similar order. By introducing the dispersive term $\mu = (\kappa_p h)^2$, in which κ_p is is the peak wavenumber given by the linear dispersion relation, and the amplitude term $\epsilon = H_{m0}/2h$, this corresponds to Ursell numbers $U_r = \epsilon/\mu$ around unity. In the following, we will only consider regions of the wave flumes where $U_r \gtrsim 0.3$.

2.3 Depth-inversion Procedure

The new depth-inversion procedure relies on the capacity of the Boussinesq theory of Herbers et al. (2002) to accurately predict the dominant wavenumbers across the shoaling and breaking wave regions (Herbers et al., 2002; Martins, Bonneton, Lannes, & Michallet, 2021). When the free surface elevation is measured, the mean water depth h is the only unknown in Equations 2-5. At each cross-shore location, h can then be retrieved through a minimisation problem, based on the match between observed κ_{obs} and predicted κ_{rms} spectra.

The mean water depth at each observation location corresponds to the depth h that minimises the following expression:

$$\sum_{\omega_i=\omega_{\min}}^{\omega_{\max}} \alpha_i \left(\kappa_{obs}(\omega_i) - \kappa_{rms}(\omega_i) \right)^2 = \sum_{\omega_i=\omega_{\min}}^{\omega_{\max}} \alpha_i \left(\kappa_{obs}(\omega_i) - \frac{\omega_i}{\sqrt{gh}} \sqrt{1 + h\gamma_{fr,1}(\omega_i) + h^2\gamma_{fr,2}(\omega_i) - \frac{1}{h}\gamma_{am}(\omega_i)} \right)^2, \tag{6}$$

where α_i are weights and $[\omega_{\min}; \omega_{\max}]$ defines the frequency range over which the minimisation is performed. Though the water depth estimates in the present study were found to be relatively insensitive to the use of frequency-dependent weights, we used the coherence obtained from the cross-spectral analyses employed to estimate κ_{obs}. In the following, we consider the range of frequencies $[0.7\omega_p; 2.5\omega_p]$, which includes the principal components (corresponding to sea/swell) and their first harmonic. This upper limit approximately corresponds to the frequency where the Boussinesq theory of Herbers et al. (2002) starts to decrease in accuracy within the nearshore region (see also Martins, Bonneton, Lannes, & Michallet, 2021).

The mean water depth estimated with the Boussinesq theory of Herbers et al. (2002) is compared with estimates from the linear wave dispersion relation (Eq. 1), which minimise the following expression:

$$\sum_{\omega_i=\omega_{\min}}^{\omega_{\max}} \alpha_i \left(h - \frac{1}{\kappa_{obs}(\omega_i)} \tanh^{-1}\left[\frac{\omega_i^2}{\kappa_{obs}(\omega_i) g} \right] \right)^2 \tag{7}$$

3 Results

3.1 Assessment of the Boussinesq Theory for Estimating Nearshore Wave Dispersive Properties

Prior to testing the new nonlinear depth-inversion approach, we first assess the capacity of the Boussinesq theory (Eq. 2) to predict the dispersive properties of irregular waves in both shoaling and breaking conditions. Fig. 2 shows the cross-shore evolution of observed and predicted dominant wave phase velocity $c(\omega) = \omega/\kappa(\omega)$ at the peak frequency ω_p (Fig 2g-i) and second harmonic $2\omega_p$ (Fig 2j-l). The significant wave height (Fig. 2a-c), as well as dispersive μ and amplitude ϵ parameters (Fig. 2d-f), are also shown since they are good indicators of the relative position in the flumes (*i.e.*, the presence of shoaling/breaking waves). In all tests considered here, wave breaking occurs at around $U_r = \epsilon/\mu \sim 1$.

The Boussinesq theory of Herbers et al. (2002) accurately predicts the cross-shore evolution of dominant wave phase velocity at both the peak frequency ω_p (Fig 2g-i) and the second harmonic $2\omega_p$ (Fig 2j-l). This confirms that the theory accurately quantifies the variation of nonlinear amplitude dispersion effects across both the shoaling region and the surf zone. At the peak frequency, deviations of observed wave phase velocities from the linear predictions steadily increase as short waves approach the breaking point and the maximum of these deviations is reached close to the shoreline for both planar beaches (up to 30% differences, see Fig 2g-h). For the barred beach, this occurs on the landward edge of the sandbar ($x \sim 14$ m), corresponding to a 10% difference (Fig 2j). At $2\omega_p$, nonlinear energy transfers between triads of frequencies (mostly self-interactions around ω_p) explain the large deviations from the linear prediction deep in the shoaling region. For the two planar beaches (Fig 2j-k), these deviations reach their maximum at locations corresponding to $U_r = \epsilon/\mu \sim 0.3 - 0.4$ and remain quite steady across both the shoaling region and surf zone (15−20% differences for both datasets). For the barred case, these differences reach 25% above the sandbar, where wave breaking is most intense ($x = 9 - 10\,\text{m}$, see Fig 2l).

Fig. 3 shows that the accuracy of the Boussinesq theory extends across the whole range of frequencies $[0.7\omega_p; 2.5\omega_p]$, which is consistent with the results of Herbers et al. (2002) and Martins, Bonneton, Lannes, and Michallet (2021). Two examples taken from the shoaling region close to the breaking point ($U_r \sim 1$) and in the surf zone ($U_r \sim 2.6 - 2.8$) are shown in Fig. 3d-f and 3g-i, respectively. As discussed in Martins, Bonneton, and Michallet (2021) for the GLOBEX case, the deviations of observed wave phase velocity spectra from linear predictions at a given frequency ω increase with the intensity of nonlinear energy transfers and the relative amount of forced energy at ω. Together with the spectral bandwidth of incident short waves (Fig. 3a-c), this explains the frequency-dependence of deviations from linear predictions observed in the shoaling region (Fig. 3e-g). In the surf zone, most components travel almost at the same velocity (Thornton & Guza, 1982; Elgar & Guza, 1985b; Martins, Bonneton, & Michallet, 2021), which explains the relatively constant observed wave phase velocity across all frequencies (Fig. 3g-i). Overall, the Boussinesq theory of Herbers et al. (2002) accurately describes the dynamics of wave fields in both shoaling and surf zone situations. For all experiments, a slight positively bias can be noted in Boussinesq predictions at frequencies corresponding to the most energetic components (up to 3-4% difference between $[0.7\omega_p; 1.5\omega_p]$, see Fig. 3d-f). This overestimation appears quite consistent across the shoaling region for the two planar cases (Fig. 2g-h).

3.2 Depth-inversion Applications

Boussinesq (Eq. 6) and linear (Eq. 7) estimates of the mean water depth h are shown in Fig. 4. These are compared against estimates obtained assuming that all incident waves propagate as fast as shallow-water waves ($c_{bulk} \sim \sqrt{gh}$) or slightly faster, due to nonlinear amplitude effects ($c_{bulk} \sim \sqrt{gh(1+\epsilon)}$). The bulk wave celerity c_{bulk} is computed through simple cross-correlation between two wave gauges (Tissier et al., 2011; Martins et al., 2016).

In both the shoaling region and the surf zone, the new Boussinesq approach substantially improves the water depth predictions compared to the linear method. For the C_3 wave test of van Noorloos (2003), the normalised error associated with the Boussinesq approach remains small ($< 10\%$), except at the early stage of the surf zone ($x = 25 - 29\,\text{m}$, see Fig. 4a and 4d). The error is generally $< 5\%$ for the most nonlinear test of GLOBEX (Fig. 4b and 4e), except at a few locations in the surf zone where it reaches $\sim 10\%$ (20% locally). This strongly contrasts with the increasing error of the linear method, which overestimates the mean water depth by over 40% across the surf zone of the planar beaches considered here. The overestimation reaches up to 80% near the shoreline for the GLOBEX case (Fig. 4b and 4e). The Boussinesq approach also performs well in the barred beach case (Fig. 4c and 4f), especially around the sandbar where mean water depths are estimated within 10% (compared to a $\sim 40 - 60\%$ overestimation with the linear approach). It is interesting to note that the beach trough section ($x = 17{-}28\,\text{m}$, Fig. 4c) corresponds to the only region for all three experiments where the linear approach outperforms the new Boussinesq approach. This is explained by the release of bound high-harmonics as short waves leave the sandbar region, a phenomenon already reported and described in the literature (*e.g.*, see Beji & Battjes, 1993; Becq-Girard et al., 1999; Masselink, 1998). In terms of wave phase velocity, this is evidenced in the close match between the observations and predictions by the linear wave dispersion at both the peak frequency (Fig. 2i) and the second harmonic (Fig. 2l).

Consistent with the large discrepancies between $\sqrt{gh}$ and the observed wave phase velocities for all experiments (Fig. 2g-l), the linear-based shallow-water predictor ($c_{bulk} \sim \sqrt{gh}$) poorly performs across both the shoaling and breaking regions considered here. Though the modified shallow water-based predictor ($c_{bulk} \sim \sqrt{gh(1+\epsilon)}$) has been observed to improve the prediction of wave phase velocities in inner surf zones (Tissier et al., 2011; Martins et al., 2018; Martins, Bonneton, & Michallet, 2021), its performance here is quite mixed. For the C_3 wave test of van Noorloos (2003), the error made on h is of similar order as the proposed Boussinesq approach, except very close to the shoreline where it reaches 20% (Fig. 4d). The performances substantially deteriorate for the A2 test during GLOBEX, where the error remains high over a large portion of the surf zone and reaches up to 40% near the shoreline (Fig. 4e). For the barred beach case (Fig. 4c and 4f), the error remains high everywhere ($\sim$ 30%), except above the sandbar where nonlinear effects are strongest (Fig. 2f).

4 Discussion and Concluding Remarks

Developing the capacity to map nearshore and surf zone bathymetry right up to the shoreline is a prerequisite to accurately quantify the morphological evolution of sandy beaches. Depth-inversion algorithms applied to remotely-sensed surface wave properties are a very promising approach to achieving this goal. However, present solutions incorporate theoretical limitations, namely, the use of the linear wave dispersion relation in regions where nonlinear effects strongly alter the dispersive properties of incident waves (*e.g.*, see Thornton & Guza, 1982; Herbers et al., 2002; Martins, Bonneton, & Michallet, 2021). Here, we present and test a new depth-inversion approach based on the stochastic Boussinesq theory of Herbers et al. (2002) for quantifying nonlinear frequency and amplitude dispersion effects and overcome these limitations.

For the relatively wide range of wave conditions and beach morphologies considered herein, the proposed Boussinesq approach results in enhanced levels of accuracy in the surf zone. Boussinesq estimates of the mean water depth are typically accurate within 10%, which substantially improves the predictions compared to the linear wave dispersion relation (errors in the range 40-80% across the surf zone). Considering frequencies just around the energy peak $[0.7\omega_p; 1.5\omega_p]$ during the minimisation procedure (Eq. 7) typically halves the error made in both the shoaling and breaking wave regions (see Fig. S3 in Supporting Information), though an 80% overestimation is still obtained at the shoreline during GLOBEX. Since the linear dispersion relation generally underestimates the peak phase velocity by typically $10-30\%$ in surf zones, this suggests that errors on the mean water depth are approximately doubled compared to those on wavenumbers, which is consistent with the analysis of Dalrymple et al. (1998). In contrast, the range of frequencies considered here only has a limited impact on the performances of the Boussinesq approach, which is explained by the accuracy of the theory at least up to $2.5\omega_p$ (Fig. 3d-i).

As for most depth-inversion algorithms, the error made on the water depth estimates has two principal sources: 1) observed $\omega - \kappa$ pairs, whose accuracy very much depends on the nature of the data; and 2) the theoretical framework for retrieving depth from those observations. Here, the main source of uncertainty on wavenumber estimates is thought to be related to the time-synchronisation of wave gauges. Imprecise time-synchronisation procedures introduces time lags related to the sampling frequency f_s (maximal lag is $0.5/f_s$), resulting in errors in wavenumber estimates. Here, we estimated that such procedures could, at most, lead to 3% errors during GLOBEX and the experiments of Michallet et al. (2011) (see Fig. S2 of Supporting Information). For the observations reported by van Noorloos (2003), the potential errors reach 10%, which is consistent with the larger errors on water depths obtained for these particular experiments. In typical field situations, where all data should be collected simultaneously, this source of error can be avoided. In the proposed Boussinesq approach, an additional source of error originates from the estimation of the nonlinear amplitude dispersion term γ_{am}. By analysing the sensitivity of depth estimates to varying levels of noise in the input signal (Fig. S1 of Supporting Information), it was found that γ_{am} is relatively insensitive to levels of noise that are realistic for lidar data collected in the field. The systematic noise in lidar data is typically two orders of magnitude lower than incident wave amplitudes, so that negligible influence of noise on the mean water depth estimates is expected.

Though bulk wave celerity can be easily estimated at large spatial scales from optical imagery in the field (*e.g.*, Lippmann & Holman, 1991), the new work presented here has highlighted the limitations of shallow-water waves predictor ($c_{bulk} \sim \sqrt{gh}$) for local depth-inversion applications. The modified predictor ($c_{bulk} \sim \sqrt{gh(1+\epsilon)}$) empirically incorporates nonlinear amplitude effects and leads to improved water depths estimation in inner surf zones, however, two main issues arise with this predictor: the accuracy appears limited under highly nonlinear conditions (Fig. 4e-f), and the seaward boundary limit where it can be used remains uncertain. Limited accuracy is thus expected when a wide range of incident wave conditions and/or beach morphology is considered. The new Boussinesq approach does not suffer from these limitations, mainly because it accurately predicts both frequency and amplitude nonlinear dispersion effects. Importantly, the proposed approach does not require any form of calibration, thus laying the basis for a universal depth-inversion relationship for nearshore and surf zone regions. The development of this new method was motivated by the recent widespread collection of high-resolution free surface elevation datasets by lidar scanners in the field (*e.g.*, Brodie et al., 2015; Martins et al., 2018; Fiedler et al., 2021). Lidar scanners have the unique feature that they directly measure both surf zone processes and the subaerial section of sandy beaches. In combination with the proposed nonlinear depth-inversion procedure, these sensors open a whole new range of possibilities for continuous monitoring of the morphological evolution of sandy beaches extending from the nearshore to the dunes.

Acknowledgments

Kévin Martins greatly acknowledges the financial support from the European Union's Horizon 2020 research and innovation program under the Marie Skłodowska-Curie Grant Agreement 887867 (*lidBathy*) that has enabled him to work with his Australian collaborators. We warmly thank Ap van Dongeren and Hervé Michallet for providing the raw data for the experiments described in van Noorloos (2003) and Michallet et al. (2011), respectively. The GLOBEX project was supported by the European Community's Seventh Framework Programme through the Hydralab IV project, EC Contract 261520. Continuous discussions over the past few years with David Lannes on Boussinesq models and methods to predict the dispersive properties of incident wave fields are greatly appreciated.

Open Research

The raw data from GLOBEX used in this research can be accessed on Zenodo at `https://zenodo.org/record/4009405` and can be used under the Creative Commons Attribution 4.0 International license. All the processed data and software produced in this study are made available to reviewers at the following link `https://filesender.renater.fr/?s=download&token=20f37b33-6a2b-44f1-be8f-26bbc75c3e91`. These will be uploaded on Zenodo upon acceptance of the manuscript in order to ensure research reproducibility and foster future efforts in improving the proposed new depth-inversion procedure.

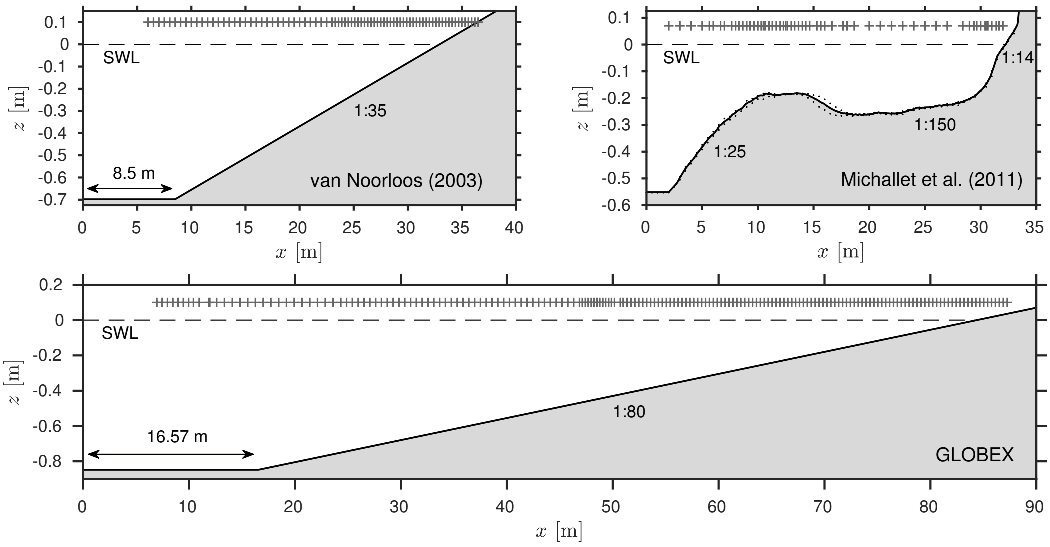

Figure 1. Beach elevation z against the cross-shore distance x for the experiments of van Noorloos (2003, top left), Michallet et al. (2011, top right) and GLOBEX (Ruessink et al., 2013, bottom). The wave paddle is located at $x = 0\,\mathrm{m}$ and grey '+' symbols show the wave gauges location. The barred beach profile for the experiments of Michallet et al. (2011) was obtained by averaging the elevations measured before and after the wave sequence, which are shown as black dotted lines (most morphological changes concentrate over the bar, $x = 7 - 18\,\mathrm{m}$).

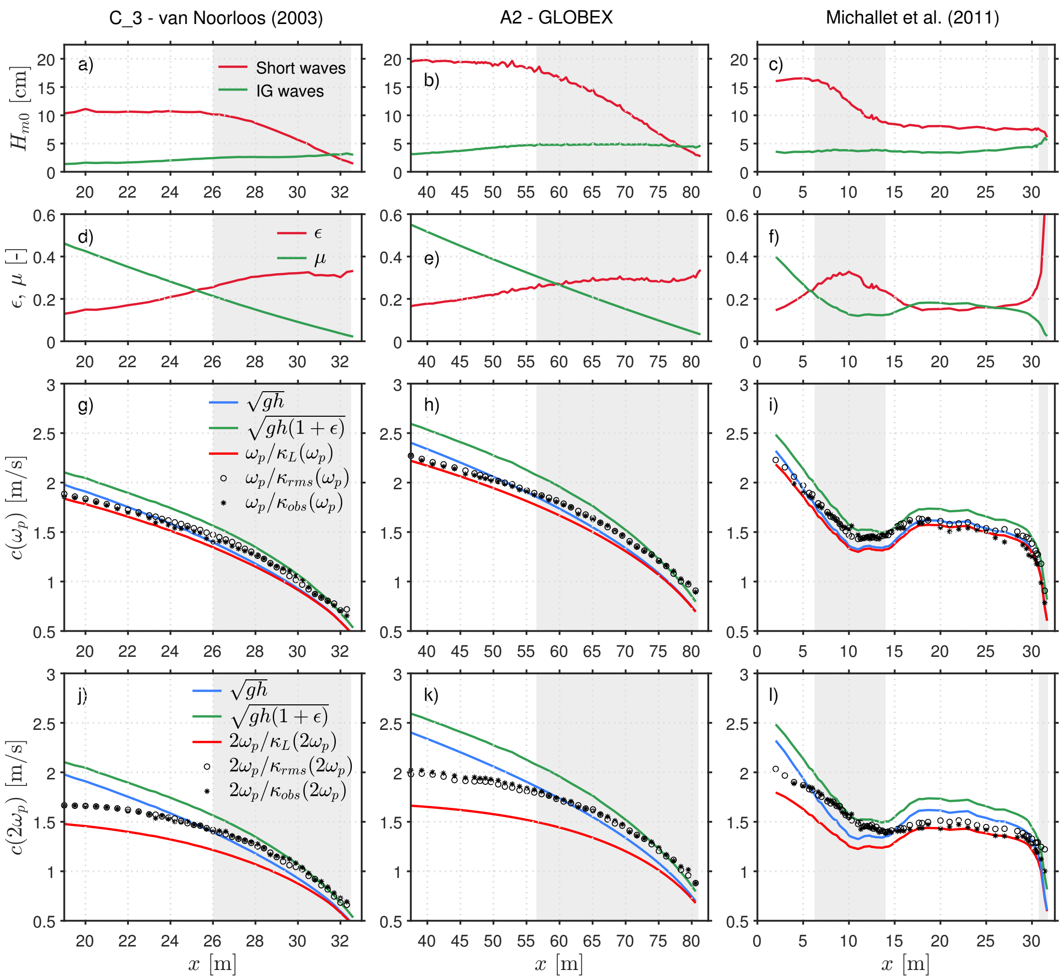

Figure 2. Assessment of the Boussinesq theory (Eq. 2) to predict the cross-shore evolution of dispersive properties during the experiments of van Noorloos (2003, left panels), GLOBEX (middle panels) and Michallet et al. (2011, right panels). Panels a-c) show the cross-shore evolution of significant wave height H_{m0} for short and infragravity (IG) waves computed as $(16\,\overline{\zeta^2})^{1/2}$ (cutoff frequency at $0.6f_p$). Panel d-f) show the amplitude ($\epsilon = H_{m0}/2h$) and dispersion ($\mu = (\kappa_p h)^2$) parameters. Panels g-j) show the observed and Boussinesq predictions of the wave phase velocity at the peak frequency ω_p, while panels k-m) show those at the second harmonic $2\omega_p$. These quantities are compared with the predictions from the linear wave dispersion (Eq. 1) and shallow-water predictors. In all panels, the grey shaded area indicates regions of the wave flume where wave breaking occurs.

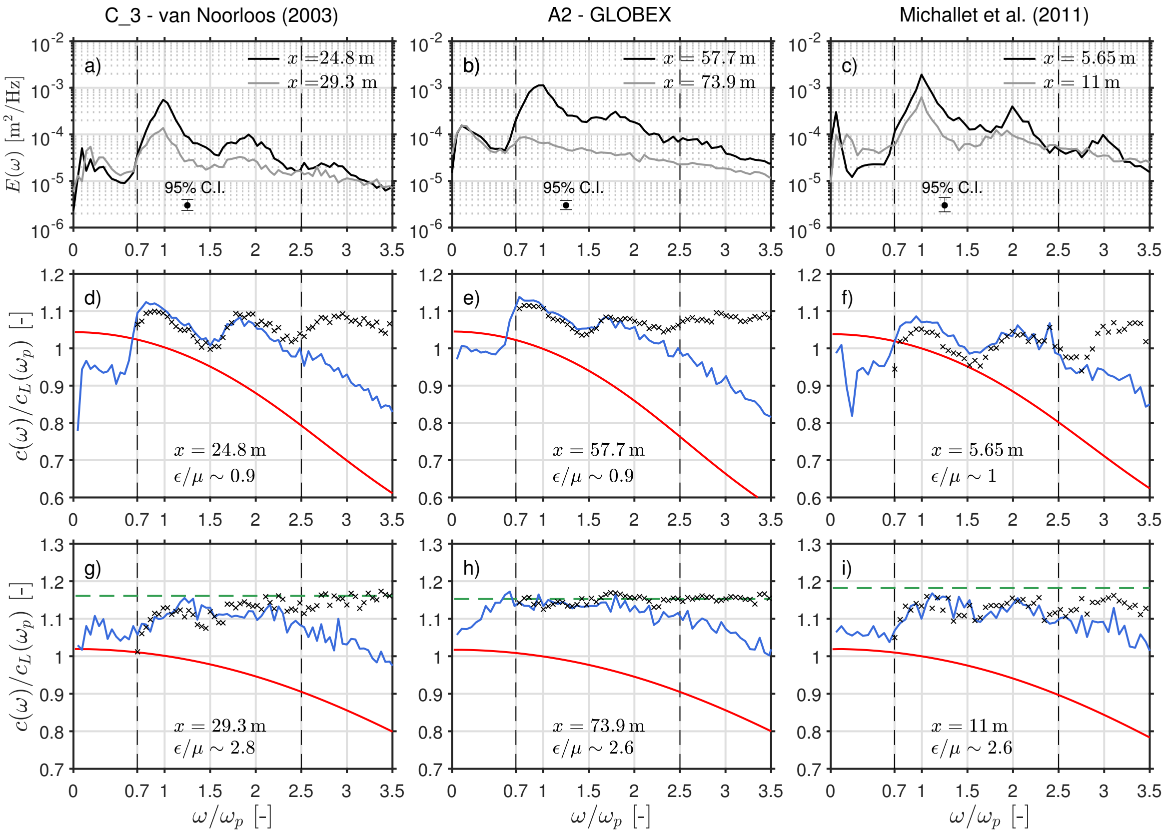

Figure 3. Assessment of the Boussinesq theory (Eq. 2) to predict wave phase spectra for the experiments of van Noorloos (2003, left panels), GLOBEX (middle panels) and Michallet et al. (2011, right panels). Panels a-c) show the energy density spectra of ζ at two positions corresponding to shoaling (panels d-f) and breaking situations (panels g-i). The normalised wave phase velocities predicted with the Boussinesq (blue lines) and linear wave (red line) theories are compared against observations (black crosses). In the surf zone (panels g-i), the green horizontal line corresponds to the modified shallow-water wave celerity predictor ($\sqrt{gh(1+\epsilon)}$). The cross-shore locations were selected based on the Ursell number ($U_r \sim 1$ and $U_r \sim 2.6 - 2.8$ for shoaling and breaking situations, respectively) and are indicated for each experiment. The vertical lines indicate the range of frequencies $[0.7\omega_p; 2.5\omega_p]$ used for the depth-inversion.

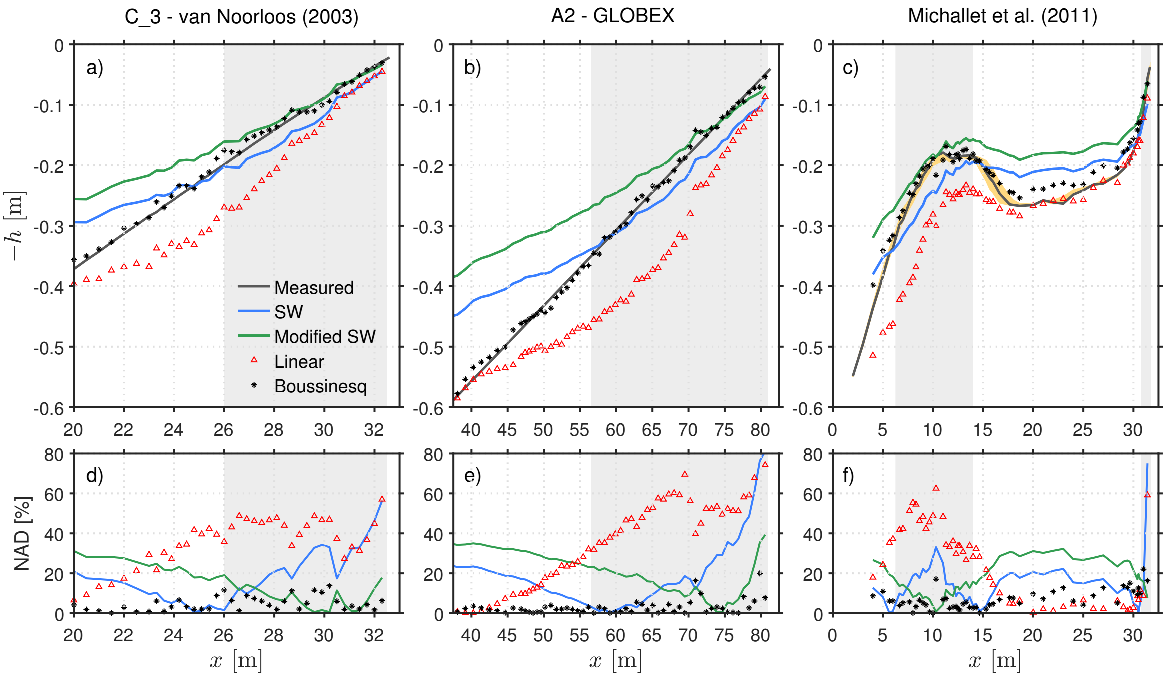

Figure 4. Results of the depth inversion applications for the experiments of van Noorloos (2003, left panels), GLOBEX (middle panels) and Michallet et al. (2011, right panels). Panels a-c) show the beach elevation profile estimated using Boussinesq (Eq. 6) and the linear wave theory (Eq. 7). These are compared with estimates based on shallow-water waves propagation velocity ('SW': $c_{bulk} \sim \sqrt{gh}$ and 'Modified SW': $c_{bulk} \sim \sqrt{gh(1+\epsilon)}$). In panel c), the orange-shaded area around the measured profile corresponds to the bed elevation changes observed during the considered wave sequence. Panel d-f) show the corresponding normalised absolute difference (NAD) of measured and predicted water depths. In all panels, the grey shaded area indicates regions of the wave flume where wave breaking occurs.

References

Becq-Girard, F., Forget, P., & Benoit, M. (1999). Non-linear propagation of unidirectional wave fields over varying topography. *Coastal Engineering*, *38*(2), 91–113. doi: 10.1016/S0378-3839(99)00043-5

Beji, S., & Battjes, J. A. (1993). Experimental investigation of wave propagation over a bar. *Coastal Engineering*, *19*(1), 151–162. doi: 10.1016/0378-3839(93)90022-Z

Bergamasco, F., Torsello, A., Sclavo, M., Barbariol, F., & Benetazzo, A. (2017). WASS: An open-source pipeline for 3D stereo reconstruction of ocean waves. *Computers & Geosciences*, *107*, 28–36. doi: 10.1016/j.cageo.2017.07.001

Bergsma, E. W. J., Almar, R., de Almeida, L. P. M., & Sall, M. (2019). On the operational use of UAVs for video-derived bathymetry. *Coastal Engineering*, *152*, 103527. doi: 10.1016/j.coastaleng.2019.103527

Bergsma, E. W. J., Conley, D. C., Davidson, M. A., & O'Hare, T. J. (2016). Video-based nearshore bathymetry estimation in macro-tidal environments. *Marine Geology*, *374*, 31–41. doi: 10.1016/j.margeo.2016.02.001

Brodie, K. L., Palmsten, M. L., Hesser, T. J., Dickhudt, P. J., Raubenheimer, B., Ladner, H., & Elgar, S. (2018). Evaluation of video-based linear depth inversion performance and applications using altimeters and hydrographic surveys in a wide range of environmental conditions. *Coastal Engineering*, *136*, 147–160. doi: 10.1016/j.coastaleng.2018.01.003

Brodie, K. L., Raubenheimer, B., Elgar, S., Slocum, R. K., & McNinch, J. E. (2015). Lidar and pressure measurements of inner-surfzone waves and setup. *Journal of Atmospheric and Oceanic Technology*, *32*(10), 1945–1959. doi: 10.1175/JTECH-D-14-00222.1

Catalán, P. A., & Haller, M. C. (2008). Remote sensing of breaking wave phase speeds with application to non-linear depth inversions. *Coastal Engineering*, *55*(1), 93–111. doi: 10.1016/j.coastaleng.2007.09.010

Dalrymple, R. A., Kennedy, A. B., Kirby, J. T., & Chen, Q. (1998). Determining depth from remotely-sensed images. In *Proceedings of the 26th Conference on Coastal Engineering, Copenhagen, Denmark* (pp. 2395–2408).

de Vries, S., Hill, D. F., de Schipper, M. A., & Stive, M. J. F. (2011). Remote sensing of surf zone waves using stereo imaging. *Coastal Engineering*, *58*(3), 239–250. doi: 10.1016/j.coastaleng.2010.10.004

Dugan, J. P., Piotrowski, C. C., & Williams, J. Z. (2001). Water depth and surface current retrievals from airborne optical measurements of surface gravity wave dispersion. *Journal of Geophysical Research: Oceans*, *106*(C8), 16903–16915. doi: 10.1029/2000JC000369

Elgar, S., & Guza, R. T. (1985a). Observations of bispectra of shoaling surface gravity waves. *Journal of Fluid Mechanics*, *161*, 425–448. doi: 10.1017/S0022112085003007

Elgar, S., & Guza, R. T. (1985b). Shoaling gravity waves: comparisons between field observations, linear theory, and a nonlinear model. *Journal of Fluid Mechanics*, *158*, 47–70. doi: 10.1017/S0022112085002543

Fiedler, J. W., Kim, L., Grenzeback, R. L., Young, A. P., & Merrifield, M. A. (2021). Enhanced surf zone and wave runup observations with hovering drone-mounted lidar. *Journal of Atmospheric and Oceanic Technology*, *38*(11), 1967–1978. doi: 10.1175/JTECH-D-21-0027.1

Freilich, M. H., Guza, R. T., & Whitham, G. B. (1984). Nonlinear effects on shoaling surface gravity waves. *Philosophical Transactions of the Royal Society of London. Series A, Mathematical and Physical Sciences*, *311*(1515), 1–41. doi: 10.1098/rsta.1984.0019

Grasso, F., Michallet, H., Barthélemy, E., & Certain, R. (2009). Physical modeling of intermediate cross-shore beach morphology: Transients and equilibrium states. *Journal of Geophysical Research: Oceans*, *114*(C9). doi: 10.1029/2009JC005308

Herbers, T. H. C., Elgar, S., Sarap, N. A., & Guza, R. T. (2002). Nonlinear dispersion of surface gravity waves in shallow water. *Journal of Physical Oceanography*, *32*(4), 1181–1193. doi: 10.1175/1520-0485(2002)032⟨1181:NDOSGW⟩2.0.CO;2

Herbers, T. H. C., Russnogle, N. R., & Elgar, S. (2000). Spectral energy balance of breaking waves within the surf zone. *Journal of Physical Oceanography*, *30*(11), 2723–2737.

Holland, T. K. (2001). Application of the linear dispersion relation with respect to depth inversion and remotely sensed imagery. *IEEE Transactions on Geoscience and Remote Sensing*, *39*(9), 2060–2072. doi: 10.1109/36.951097

Holman, R., & Bergsma, E. W. J. (2021). Updates to and performance of the cbathy algorithm for estimating nearshore bathymetry from remote sensing imagery. *Remote Sensing*, *13*(19). doi: 10.3390/rs13193996

Holman, R., Plant, N., & Holland, T. (2013). cBathy: A robust algorithm for estimating nearshore bathymetry. *Journal of Geophysical Research: Oceans*, *118*(5), 2595–2609. doi: 10.1002/jgrc.20199

Lippmann, T. C., & Holman, R. A. (1991). Phase speed and angle of breaking waves measured with video techniques. In *Proceedings of Coastal Sediments '91, American Society of Civil Engineers, New York* (pp. 542–556).

Martins, K., Blenkinsopp, C. E., Deigaard, R., & Power, H. E. (2018). Energy dissipation in the inner surf zone: New insights from lidar-based roller geometry measurements. *Journal of Geophysical Research: Oceans*, *123*(5), 3386–3407. doi: 10.1029/2017JC013369

Martins, K., Blenkinsopp, C. E., Power, H. E., Bruder, B., Puleo, J. A., & Bergsma, E. W. J. (2017). High-resolution monitoring of wave transformation in the surf zone using a LiDAR scanner array. *Coastal Engineering*, *128*, 37–43. doi: 10.1016/j.coastaleng.2017.07.007

Martins, K., Blenkinsopp, C. E., & Zang, J. (2016). Monitoring individual wave characteristics in the inner surf with a 2-dimensional laser scanner (LiDAR). *Journal of Sensors, 2016*, 1–11. doi: 10.1155/2016/7965431

Martins, K., Bonneton, P., Lannes, D., & Michallet, H. (2021). Relation between orbital velocities, pressure, and surface elevation in nonlinear nearshore water waves. *Journal of Physical Oceanography*, *51*(11), 3539–3556. doi: 10.1175/JPO-D-21-0061.1

Martins, K., Bonneton, P., & Michallet, H. (2021). Dispersive characteristics of nonlinear waves propagating and breaking over a mildly sloping laboratory beach. *Coastal Engineering*, *167*, 103917. doi: 10.1016/j.coastaleng.2021.103917

Masselink, G. (1998). Field investigation of wave propagation over a bar and the consequent generation of secondary waves. *Coastal Engineering*, *33*(1), 1–9. doi: 10.1016/S0378-3839(97)00032-X

Michallet, H., Cienfuegos, R., Barthélemy, E., & Grasso, F. (2011). Kinematics of waves propagating and breaking on a barred beach. *European Journal of Mechanics - B/Fluids*, *30*(6), 624–634. doi: 10.1016/j.euromechflu.2010.12.004

Phillips, O. M. (1960). On the dynamics of unsteady gravity waves of finite amplitude. Part 1. The elementary interactions. *Journal of Fluid Mechanics*, *9*(2), 193–217. doi: 10.1017/S0022112060001043

Plant, N. G., Holland, K. T., & Haller, M. C. (2008). Ocean wavenumber estimation from wave-resolving time series imagery. *IEEE Transactions on Geoscience and Remote Sensing*, *46*(9), 2644–2658. doi: 10.1109/TGRS.2008.919821

Ruessink, G. B., Michallet, H., Bonneton, P., Mouazé, D., Lara, J. L., Silva, P. A., & Wellens, P. (2013). GLOBEX: Wave dynamics on a gently sloping laboratory beach. In *Coastal Dynamics '13: Proceedings of the Seventh Conference on Coastal Dynamics, Arcachon, France.*

Stockdon, H. F., & Holman, R. A. (2000). Estimation of wave phase speed and nearshore bathymetry from video imagery. *Journal of Geophysical Research: Oceans*, *105*(C9), 22015–22033. doi: 10.1029/1999JC000124

Thornton, E. B., & Guza, R. T. (1982). Energy saturation and phase speeds measured on a natural beach. *Journal of Geophysical Research*, *87*(C12), 9499–9508. doi: 10.1029/JC087iC12p09499

Tissier, M., Bonneton, P., Almar, R., Castelle, B., Bonneton, N., & Nahon, A. (2011). Field measurements and non-linear prediction of wave celerity in the surf zone. *European Journal of Mechanics - B/Fluids*, *30*(6), 635–641. doi: 10.1016/j.euromechflu.2010.11.003

van Dongeren, A., Battjes, J., Janssen, T., van Noorloos, J., Steenhauer, K., Steenbergen, G., & Reniers, A. (2007). Shoaling and shoreline dissipation of low-frequency waves. *Journal of Geophysical Research: Oceans*, *112*, C02011. doi: 10.1029/2006JC003701

van Noorloos, J. C. (2003). *Energy transfer between short wave groups and bound long waves on a plane slope* (Master's thesis, Delft University of Technology, Delft, The Netherlands). Retrieved from http://resolver.tudelft.nl/uuid:13616ff0-407d-43de-9954-ba707cd40d27

Supporting Information for:

New Perspectives for Nonlinear Depth-inversion of the Nearshore Using Boussinesq Theory

Kévin Martins[1,2], Philippe Bonneton[1], Olivier de Viron[3], Ian L. Turner[2], Mitchel D. Harley[2], Kristen Splinter[2]

[1]Univ. Bordeaux, CNRS, Bordeaux INP, EPOC, UMR 5805, F-33600 Pessac, France
[2]Water Research Laboratory, School of Civil and Environmental Engineering, UNSW Sydney, 110 King Street, Manly Vale, NSW, 2093, Australia
[3]La Rochelle University, CNRS, LIENSs, UMRi 7266, 17000 La Rochelle, France

1 Introduction

This Supporting Information contains additional details on the quantification of uncertainties on the mean water depths estimated with the new Boussinesq depth-inversion procedure. This is primarily intended to support the discussion points and conclusions of the study as provided in Section 4 of the manuscript. Below, additional information on the spectral analyses is first given (Section 2). We then provide an analysis on the sensitivity of depth estimates to the observations used for the inversion procedure. The sensitivity to spectral and bispectral estimates, which are used to quantify non-linear amplitude dispersion effects, are analysed in Section 3.1 by adding varying levels of white noise to the timeseries of free surface elevation ζ. The uncertainty on observed wavenumbers and the associated error on water depth estimates are analysed in Section 3.2 by quantifying the effect of potential time lags originating from the synchronisation process on the computation of wave phase speeds at the peak frequency. Finally, the depth-inversion results obtained using only the range of frequencies corresponding to the most energetic components ($[0.7\omega_p, 1.5\omega_p]$) are given in Section 4.

2 Definition and computation of spectral products

At the basis of the depth-inversion procedure, dominant wavenumber spectra κ_{obs} are estimated using cross-spectral analyses following Martins et al. (2021). Let C_{x_1,x_2} denote the cross-spectrum computed from the surface elevation signal ζ measured at two adjacent gauges located at positions x_1 and x_2:

$$C_{x_1,x_2}(\omega) = \mathcal{E}\left[A_{x_1}(\omega)\, A^*_{x_2}(\omega)\right], \tag{1}$$

where $\omega = 2\pi f$ is the angular frequency, A are the complex Fourier coefficients of ζ at the corresponding locations, * denotes the complex conjugate and $\mathcal{E}$ is an expected, or ensemble-average, value. The coherence $\mathrm{coh}(\omega)$ and phase $\phi(\omega)$ spectra computed between x_1 and x_2 are then given by:

$$\begin{aligned} \mathrm{coh}_{\mathrm{x_1,x_2}}(\omega) &= \left[\frac{C_{x_1,x_2}(\omega)\, C^*_{x_1,x_2}(\omega)}{C_{x_1,x_1}(\omega)\, C_{x_2,x_2}(\omega)}\right]^{1/2} & (2)\\ \phi_{x_1,x_2}(\omega) &= \arctan\left[\frac{\mathrm{Im}\{C_{x_1,x_2}(\omega)\}}{\mathrm{Re}\{C_{x_1,x_2}(\omega)\}}\right], & (3) \end{aligned}$$

where $\mathrm{Re}\{\cdot\}$ and $\mathrm{Im}\{\cdot\}$ are the real and imaginary parts of the cross-spectra, respectively. The time delay (in sec) per frequency is obtained from the unwrapped phase ϕ^{unw} which,

Corresponding author: Kévin Martins, kevin.martins@u-bordeaux.fr

in the case of progressive waves propagating in one dimension, is easily retrieved from phase jumps. The wavenumber $\kappa(\omega)$ and (cross-shore) phase velocity $c(\omega)$ spectra are then readily computed as:

$$\kappa(\omega) = \phi^{unw}_{x_1,x_2}(\omega) \,/\, \Delta x \tag{4}$$
$$c(\omega) = \omega \Delta x \,/\, \phi^{unw}_{x_1,x_2}(\omega), \tag{5}$$

where Δx is the spacing between the two wave gauges. κ refers to the single-valued wavenumber modulus and is representative of the energy spread across both forced and free components at a given frequency (Herbers et al., 2002; Martins et al., 2021). In practice, κ and c provide estimates at $x = (x_1+x_2)/2$ of the dominant wavenumber (in an energy-averaged sense) and the corresponding propagation velocity, respectively. Cross-spectra are here computed using Welch's method and Hann-windowed blocks of 128 seconds, which were overlapping by 75%. This results in each spectral estimate having approximately 51, 71 and 30 equivalent degrees of freedom for the datasets of van Noorloos (2003), GLOBEX and Michallet et al. (2011), respectively, while a spectral resolution of 0.0078 Hz is retrieved in all cases.

Let E and B denote the spectral and bispectral densities of the free surface elevation signal ζ, respectively. The energy spectra E is here given by:

$$E(\omega) = 2\,\mathcal{E}\left[A(\omega)\,A^*(\omega)\right], \tag{6}$$

The bispectrum of ζ is here computed following Kim and Powers (1979) as:

$$B(\,\omega_1,\,\omega_2) = \mathcal{E}\left[A(\omega_1)\,A(\omega_2)\,A^*(\omega_1+\omega_2)\right], \tag{7}$$

Both energy spectra and bispectra of ζ are computed using 128 s blocks overlapping by 75%. Statistical stability of bispectra is increased by merging estimates over three frequencies (Elgar & Guza, 1985). This results in bispectral estimates having approximately 90, 149 and 55 equivalent degrees of freedom during the experiments of van Noorloos (2003), GLOBEX and Michallet et al. (2011), respectively, with a spectral resolution of 0.023 Hz for all experiments.

3 Sensitivity of Depth Estimates to Observations

3.1 Computation of Bispectral Products

In the new Boussinesq depth-inversion method described in the manuscript, dominant wavenumber spectra κ_{rms} are estimated from ζ as follows (Herbers et al., 2002):

$$\kappa_{rms}(\omega) = \frac{\omega}{\sqrt{gh}}\sqrt{1 + h\gamma_{fr,1}(\omega) + h^2\gamma_{fr,2}(\omega) - \frac{1}{h}\gamma_{am}(\omega)}, \tag{8}$$

with

$$\gamma_{fr,1}(\omega) = \frac{\omega^2}{3g} \tag{9}$$
$$\gamma_{fr,2}(\omega) = \frac{\omega^4}{36g^2} \tag{10}$$
$$\gamma_{am}(\omega) = \frac{3}{2E(\omega)}\int_{-\infty}^{\infty} \mathrm{Re}\{B(\omega', \omega-\omega')\}d\omega', \tag{11}$$

where g is the acceleration of gravity, h is the mean water depth and Re{.} denotes the real part.

In contrast with linear theory-based depth-inversion algorithms, which do not estimate non-linear amplitude effects, the estimation of γ_{am} leads to an additional source of uncertainty in the final water depth estimate through computations of E and B. The sensitivity of the water depth estimates to the computation of spectral and bispectral products was here analysed by adding varying levels of white noise to the free surface elevation signal ζ. Fig. S1 gathers the results of this sensitivity analysis performed at the two locations corresponding to shoaling and breaking situations used in the manuscript. For each level of signal-to-noise ratio (SNR), the analysis was repeated 200 times, and results are shown in terms of deviation from the measured mean water depth value h_{obs}: $\delta_h = (h - h_{obs})/h_{obs} \times 100$. The development of the present depth-inversion methodology was motivated and designed for future use in the field using highly-resolved free surface elevation datasets. At the moment, lidar scanners offer the most robust and promising solution, but the new depth-inversion approach can be applied to any technology capable of collecting high-resolution free surface elevation datasets (*e.g.*, stereo-video imagery). Though this might vary between field deployments and lidar scanner models, the systematic noise in lidar data does not generally exceed a few centimeters, which is 1-2 orders of magnitude lower than the amplitude of incident waves typically measured in the field (Brodie et al., 2015; Martins et al., 2016; Fiedler et al., 2021). Thus, it is worth noting that SNR associated with typical lidar deployments should typically be above 20. Here, the estimation of γ_{am} was hence found little sensitive to realistic levels of noise for lidar data collection in the field (Fig. S1). For instance, a SNR of 20 has negligible effects on the water depth estimates, with deviations of mean water depths within 1%. The predicted water depths rapidly increase for SNR lower than 15 and, though considered unrealistic, a SNR of 10 for instance leads to water depth estimates that deviate by up to 2% and 4% compared to a situation without noise in shoaling and breaking situations, respectively. Since bispectra only reflect non-linear couplings within a signal, the influence of the added noise mostly biases low γ_{am} (hence bias high h) by overestimating the variance of the signal (see Eq. 11).

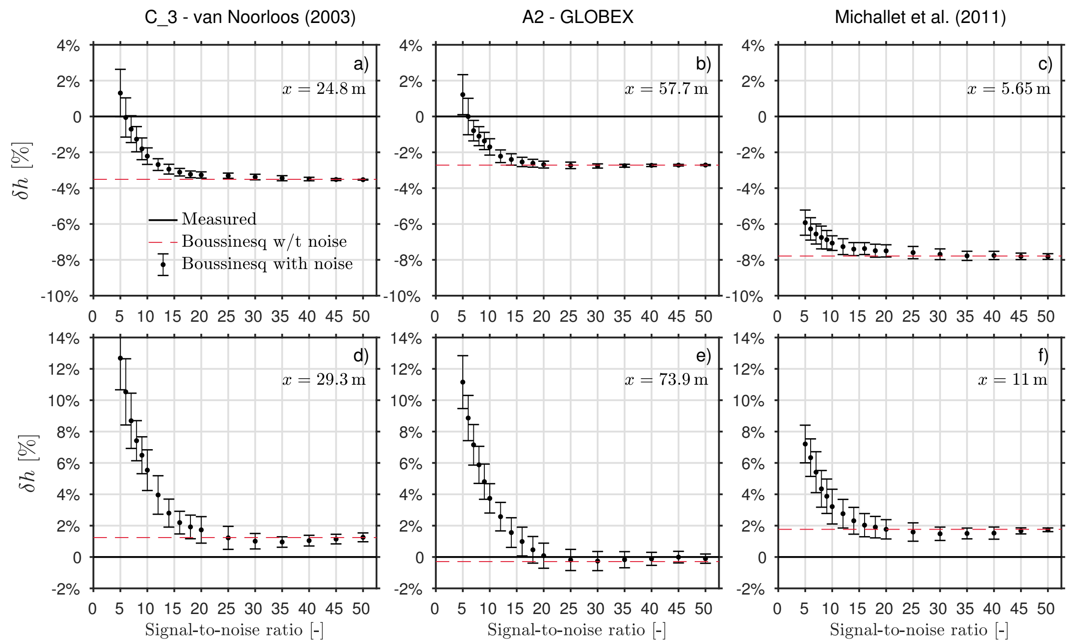

Figure S1. Sensitivity of mean water depths estimates to the computation of non-linear amplitude dispersion effects (γ_{am} in Eq. 11) at two cross-shore locations corresponding to shoaling (top panels) and breaking (bottom panels) situations. Boussinesq estimates of the mean water depths are shown in terms of deviation from the observed value h_{obs}: $\delta_h = (h - h_{obs})/h_{obs} * 100$. The error bar corresponds to the standard deviation obtained for the 200 repetitions performed.

3.2 Estimation of Wave Dominant Dispersive Properties

In order to collect surface elevation data at high spatial resolution in the considered experiments, each wave test was repeated several times and wave gauges were displaced along the different wave flumes. A cross-correlation technique applied on waves gauges held at a fixed position in the flume is then typically used to achieve the time-synchronisation between the signals from all wave gauges (*e.g.*, see van Noorloos, 2003). This approach leads to an error on the time correction that is bounded by the sampling frequency f_s, *i.e.* errors up to $0.5/f_s$ can be made locally. In the surf zone during the experiments of van Noorloos (2003), with a spatial resolution of 0.3 m, this represents up to 5% of the time taken by a wave component around the peak frequency to travel between two wave gauges. The time-synchronisation is thus believed to be a non-negligible source of errors in the estimations of the mean water depth. The effect of potential time lags on the final estimate of the mean water depth is investigated here at the peak frequency by adjusting the observed wavenumber κ_{obs} in the depth-inversion procedure. The results are shown in Fig. S2 in terms of deviation from the value predicted without adjustments. As expected, the effect of potential time lags due to errors in the synchronisation process is greatest for the dataset from the experiments of van Noorloos (2003) due to the lower sampling rate (20 Hz, instead of 100 Hz for GLOBEX and 50 Hz for the experiments of Michallet et al., 2011). For all experiments, the variations in mean water depth estimates obtained for realistic variations of the wave propagation velocity is relatively large compared to the errors obtained. Though it is hard to estimate how likely such time lags were introduced, we suspect that they explain a substantial fraction of the errors obtained on the mean water depths estimates in this study, especially at localised spikes (*e.g.*, see around $x = 26, 30$ m in Fig. 4a and 4d, $x = 71$ m in Fig. 4b and 4e and $x = 10$ m in Fig. 4c and 4f of the manuscript).

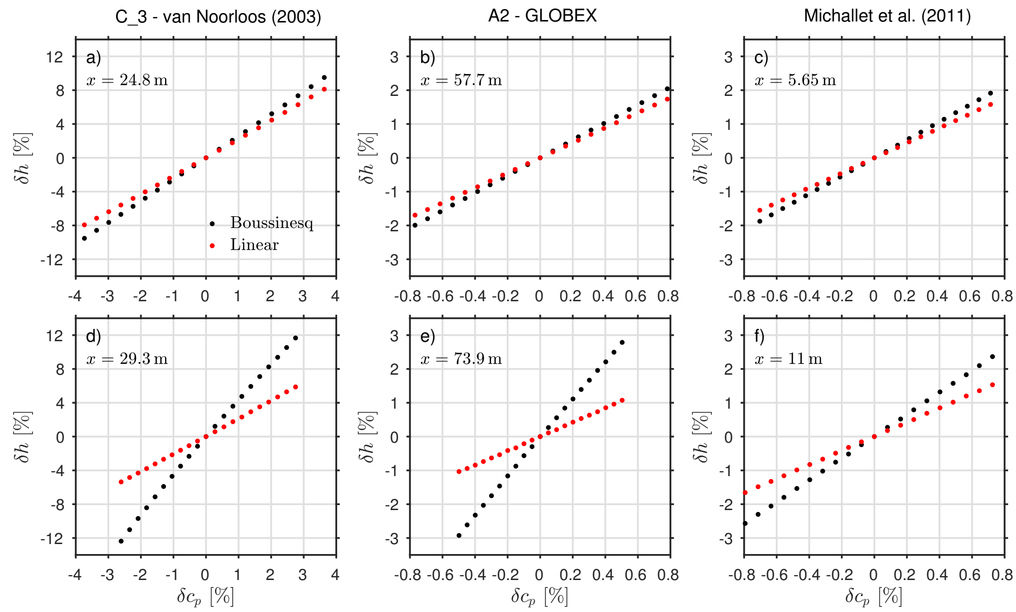

Figure S2. Sensitivity of mean water depths estimates to potential time lags introduced during the synchronisation process at two cross-shore locations corresponding to shoaling (top panels) and breaking (bottom panels) situations. Results are shown in terms of deviation of mean water depth estimate from the value estimated without adjustments as a function of the adjustments made to the observations (here the wave phase velocity at the peak frequency c_p). The adjustments made to the peak wave velocity are bounded by both the sampling frequency and spatial resolution characterising each experiment.

4 Depth-inversion Using Most Energetic Components

The full range of frequencies $[0.7\omega_p; 2.5\omega_p]$ is presently used during the minimisation procedure for estimating the mean water depth (Eq. 7-8 of the companion manuscript). Fig. S3 shows the depth-inversion results obtained when only frequencies within $[0.7\omega_p; 1.5\omega_p]$ are considered, *i.e.* taking only the most energetic components of the wave field. As briefly discussed in the manuscript, only accounting for the most energetic wave components substantially reduces the error made with the linear approach, which is explained by the increasing deviations of wavenumbers predicted by the linear wave dispersion from observations as frequencies increase (Fig. 3 of the manuscript). An important remark to be made here is that using only frequencies within $[0.7\omega_p; 1.5\omega_p]$ corresponds to the minimal error that can be reached with a linear approach, since the error on mean water depth estimates are expected to grow with the number of super-harmonics considered. For the planar beach cases, the error reduces from around 30−40% to 10% just seaward of the surf zone. Except close to the shoreline during GLOBEX, where the error remains around 80% for both frequency ranges, considering only frequencies within $[0.7\omega_p; 1.5\omega_p]$ typically halves the error made in the surf zone for all cases. In shallow water depths ($\mu \lesssim 0.1$, see Fig. 2d-f of the manuscript), it is worth noting that the water depth estimates obtained with the linear approach and the shallow-water wave celerity predictor ($c_{bulk} \sim \sqrt{gh}$) converge towards the same value. This is explained by the fact that in shallow water, $\sqrt{gh}$ provides a good estimate of the peak wave phase velocity.

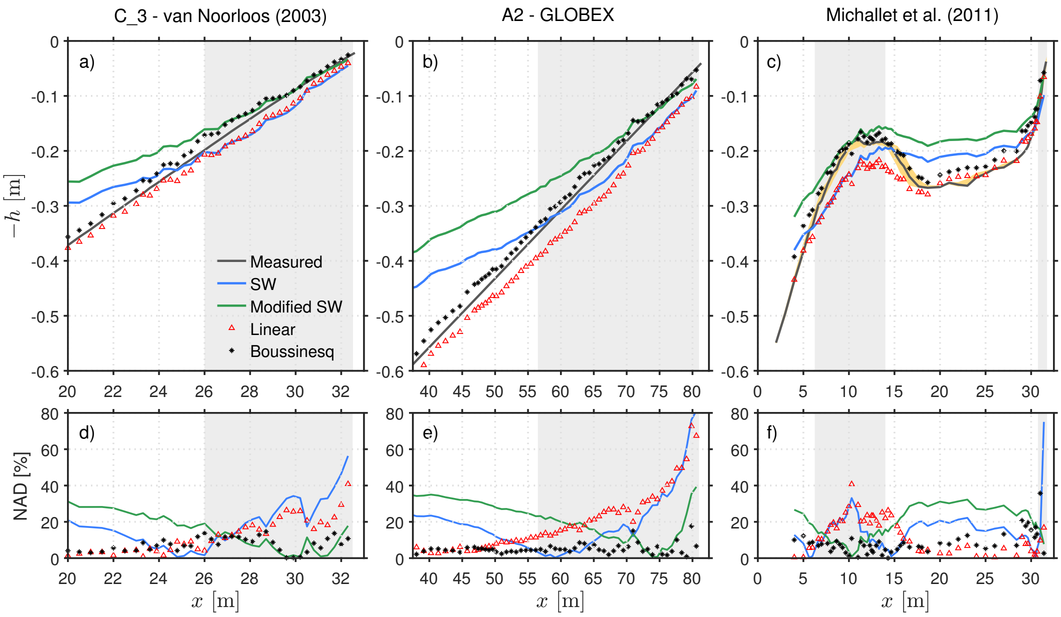

Figure S3. Results of the depth inversion applications over the range of frequencies $[0.7\omega_p; 1.5\omega_p]$ for the experiments of van Noorloos (2003) (left panels), GLOBEX (middle panels) and Michallet et al. (2011) (right panels). Panels a-c) show the beach elevation profile estimated using Boussinesq and the linear wave theory. These are compared with estimates based on shallow-water waves propagation speed ('SW': $c_{bulk} \sim \sqrt{gh}$ and 'Modified SW': $c_{bulk} \sim \sqrt{gh(1+\epsilon)}$). In panel c), the orange-shaded area around the measured profile corresponds to the bed elevation changes observed during the considered wave sequence. Panel d-f) show the corresponding normalised absolute difference (NAD), computed between measured and predicted water depths. In all panels, the grey shaded area indicates regions of the wave flume where wave breaking occurs.

References

Brodie, K. L., Raubenheimer, B., Elgar, S., Slocum, R. K., & McNinch, J. E. (2015). Lidar and pressure measurements of inner-surfzone waves and setup. *Journal of Atmospheric and Oceanic Technology*, *32*(10), 1945–1959. doi: 10.1175/JTECH-D-14-00222.1

Elgar, S., & Guza, R. T. (1985). Observations of bispectra of shoaling surface gravity waves. *Journal of Fluid Mechanics*, *161*, 425–448. doi: 10.1017/S0022112085003007

Fiedler, J. W., Kim, L., Grenzeback, R. L., Young, A. P., & Merrifield, M. A. (2021). Enhanced surf zone and wave runup observations with hovering drone-mounted lidar. *Journal of Atmospheric and Oceanic Technology*, *38*(11), 1967–1978. doi: 10.1175/JTECH-D-21-0027.1

Herbers, T. H. C., Elgar, S., Sarap, N. A., & Guza, R. T. (2002). Nonlinear dispersion of surface gravity waves in shallow water. *Journal of Physical Oceanography*, *32*(4), 1181–1193. doi: 10.1175/1520-0485(2002)032⟨1181:NDOSGW⟩2.0.CO;2

Kim, Y. C., & Powers, E. J. (1979). Digital Bispectral Analysis and Its Applications to Nonlinear Wave Interactions. *IEEE Transactions on Plasma Science*, *7*(2), 120–131. doi: 10.1109/TPS.1979.4317207

Martins, K., Blenkinsopp, C. E., & Zang, J. (2016). Monitoring individual wave characteristics in the inner surf with a 2-dimensional laser scanner (LiDAR). *Journal of Sensors, 2016*, 1–11. doi: 10.1155/2016/7965431

Martins, K., Bonneton, P., & Michallet, H. (2021). Dispersive characteristics of nonlinear waves propagating and breaking over a mildly sloping laboratory beach. *Coastal Engineering*, *167*, 103917. doi: 10.1016/j.coastaleng.2021.103917

Michallet, H., Cienfuegos, R., Barthélemy, E., & Grasso, F. (2011). Kinematics of waves propagating and breaking on a barred beach. *European Journal of Mechanics - B/Fluids*, *30*(6), 624–634. doi: 10.1016/j.euromechflu.2010.12.004

van Noorloos, J. C. (2003). *Energy transfer between short wave groups and bound long waves on a plane slope* (Unpublished master's thesis). Delft University of Technology, Delft, The Netherlands.